Paper

# An Efficiency Optimization Method of Static Wireless Power Transfer Coreless Coils for Electric Vehicles in the 85 kHz Band Using Numerical Analysis

Yuto Yamada[a], Student Member
Takehiro Imura, Member

Wireless power transfer (WPT) has been attracting a lot of attention in recent years for its ability to greatly improve the convenience of our lives. Moreover, WPT for Electric Vehicles (EVs) has become an important key to the spread of EVs. The efficiency of WPT using magnetic field resonant coupling can be evaluated by the $kQ$ product, but the optimal coil design method to maximize the $kQ$ product at a specific frequency has not yet been established. In this paper, taking the Test station GA-WPT1 and the Test station VA-WPT1/Z3 of SAE J2954, which is officially defined as the standard for WPT while the electric vehicle is stationary in October 2020, as examples, the coil parameters that maximize the $kQ$ product in the case of the coreless are determined according to the proposed method. An efficiency of 99.13% was obtained with a transmission distance of 200 mm and the number of turns of $N_1 = 34$ and $N_2 = 30$. Also, since all analyses can be derived immediately except for the analysis of the Litz wire to be used, the optimization time could be reduced significantly compared with the electromagnetic field analysis.

**Keywords:** wireless power transfer; electric vehicle; coil design; SAE J2954; SWPT

*Received 27 September 2021; Revised 18 May 2022*

## 1. Introduction

Research on wireless power transfer (WPT), which can charge any device without cables, is very prominent [1]. In recent years, many countries have banned the sale of new internal combustion engine (ICE) vehicles, and electric vehicles, which do not emit greenhouse gases during driving, are expected to attract more attention. The use of stationary WPT in electric vehicles will improve convenience and prevent electric shock accidents by eliminating the need for charging plugs [2,3]. In addition, research is being conducted on Dynamic Wireless Power Transfer (DWPT), in which power is supplied from the road while the vehicle is driving [4–8]. Several papers have discussed the limitations of lithium-ion batteries [9,10], and DWPT is very attractive because it can reduce the size of the on-board battery, reduce the price of the EV, and theoretically achieve unlimited range [11]. Although there are some concerns that the amount of power generation will not be able to keep up with the spread of electric vehicles [12], the future of WPT research is bright, as it is being considered to be combined with solar power generation [13,14]. Since there are many technical issues between power transfer while the vehicle is parking and power supply while the vehicle is driving, quasi-driving power supply technology is also being studied, in which power is supplied when the vehicle is stopped at a traffic signal [15]. As a result, WPT in electric vehicles is attracting a lot of attention as a clue to the spread of electric vehicles [16–18]. There are several methods of WPT, such as magnetic field coupling, electric field coupling, microwave, and laser, but the magnetic field resonance method with resonant capacitors attached to the coils on the transmission and receiving sides is adopted for WPT in electric vehicles because it has a large air gap (This term means transmission distance), is resistant to misalignment, and can apply a large amount of power.

The efficiency of WPT using magnetic field resonant coupling can be evaluated by the $kQ$ product using the coupling coefficient $k$ between coils and the $Q$ value of the coil, but the optimal coil design method to maximize the $kQ$ product at a specific frequency has not yet been established.

In the previous research, electromagnetic field analysis is mainly conducted using finite element method (FEM) [19–22], but it is very time-consuming because the parameters of coils and Litz wires are changed one by one and better coils are sought by trial and error. Some methods such as particle swarm optimization (PSO) are available, but they require a large analysis computer, while the proposed method can be easily performed on a laptop computer.

As a coil design, it is necessary to consider the material [23], coating [21], and twist pitch selection of the Litz wire [24] to be used, as well as the optimization of the entire system [25], including the power supply, inverter, and rectifier, but this paper focuses on the coupler section and does not consider it in order to systematically show the coil design procedure.

In this paper, we take the Test station GA-WPT1 (580 mm × 420 mm) shown in Fig. 1 and the Test station VA-WPT1 (420 mm × 420 mm)/Z3 (air gap 200 mm) shown in Fig. 2 as

[a] Correspondence to: Yuto Yamada. E-mail: yuto.yamada20@gmail.com

Tokyo University of Science, Factory and Engineering, Imura Laboratory, Noda, Chiba, Japan

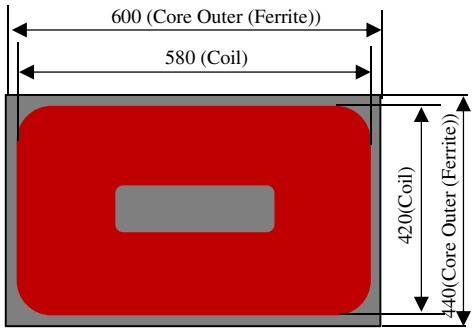


Fig. 1. Test station GA-WPT1

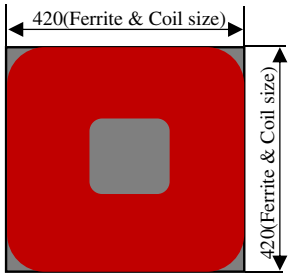


Fig. 2. Test station VA-WPT1/Z3

examples of SAE J2954 [26], which is officially defined as the standard for power transfer at stationary in October 2020.

Using Litz wires which the number of strands is 4000, we propose the best coil design for more practical conditions where coil size is required.

Section 2 presents the relational equation for the magnetic field resonant coupling (S−S) method, Section 3 shows how to derive the parameters used, Section 4 shows the optimization procedure and experimental results, and Section 5 provides a conclusion.

## 2. Derivation of the Theoretical Equation for the S−S Method

### 2.1. Derivation of efficiency of equivalent circuit

In this paper, the S−S (Series−Series) magnetic field resonance method is used to connect the resonant capacitor in series with the coil on both the transmission (primary) and the receiving (secondary) sides [27]. The equivalent circuit is shown in Fig. 3. The parameters are the internal resistance of the transmission and receiving coils $r_1$ and $r_2$, the self-inductance of the transmission and receiving coils $L_1$ and $L_2$, each resonant capacitor $C_1$ and $C_2$, and the load resistance $R_L$. Since the reactance due to the self-inductance $L_1$ and $L_2$ and the reactance due to the capacitance $C_1$ and $C_2$ cancel each other out under the resonance condition, the resonance angular frequency $\omega_0$ can be expressed as follows

$$\omega_0 = 2\pi f = \frac{1}{\sqrt{L_1 C_1}} = \frac{1}{\sqrt{L_2 C_2}} \tag{1}$$

Using (1), the efficiency of the circuit $\eta$ can be expressed as (2).

$$\eta = \frac{R_L(\omega_0 L_m)^2}{(r_2 + \mathrm{R_L})\left\{r_1 (r_2 + R_L) + (\omega_0 L_m)^2\right\}} \tag{2}$$

The maximum efficiency in (2) is obtained when the optimum load $R_{L,\eta max}$, derived using the conditional equation in (3), is applied. The equations for the optimum load $R_{L,\eta max}$ and the maximum efficiency $\eta_{max}$ are shown in (4) and (5).

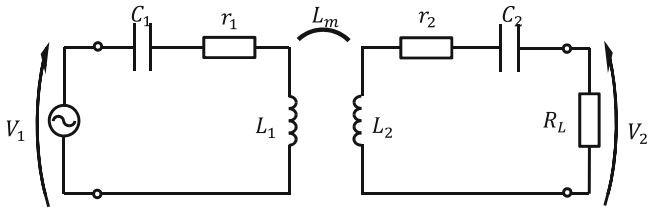


Fig. 3. Equivalent circuit in magnetic field resonance coupling of (S−S)

$$\frac{\partial \eta}{\partial R_L} = 0 \tag{3}$$

$$R_{L,\eta max} = r_2\sqrt{1 + \frac{(\omega_0 L_m)^2}{r_1 r_2}} \tag{4}$$

$$\eta_{max} = \frac{(\omega_0 L_m)^2}{\left(\sqrt{r_1 r_2} + \sqrt{r_1 r_2 + (\omega_0 L_m)^2}\right)^2} \tag{5}$$

### 2.2. Derivation of the $kQ$ product

The coupling coefficient $k$, which indicates the degree of coupling of the coil, can be expressed by (6) using the inductance $L_1$, $L_2$ and mutual inductance $L_m$ of the primary and secondary coils. The $Q$ value, which indicates the quality of the coil, can be expressed as (7) using the internal resistance of the coil $r_i$ $(i = 1, 2)$ and the self-inductance $L_i$ $(i = 1, 2)$.

Now, using (6) and (7), the $kQ$ product can be expressed as (8).

$$k = \frac{L_m}{\sqrt{L_1 L_2}} \tag{6}$$

$$Q = \frac{\omega_0 L_i}{r_i} \tag{7}$$

$$k^2 Q_1 Q_2 = \frac{(\omega_0 L_m)^2}{r_1 r_2} \tag{8}$$

The value obtained by taking the square root of (8) is sometimes referred to as the $kQ$ product, but in this paper, the $kQ$ product is expressed as an equation without square root for simplicity of calculation. Equations (6) and (7) can be expressed as (9) and (10) by using the coupling coefficient $k$ and $Q$ value.

$$R_{L,\eta max} = r_2\sqrt{1 + k^2 Q_1 Q_2} \tag{9}$$

$$\eta_{max} = \frac{k^2 Q_1 Q_2}{\left(1 + \sqrt{1 + k^2 Q_1 Q_2}\right)^2} \tag{10}$$

$$P_2 = \frac{R_L(\omega_0 L_m)^2}{\left\{r_1 (r_2 + R_L) + (\omega_0 L_m)^2\right\}^2} V_1^2 \tag{11}$$

From (10), the efficiency $\eta_{max}$ is a monotonic increase in the $kQ$ product. In this paper, in order to study the optimization of WPT coils in the 85 kHz band, the transmission efficiency $\eta_{max}$ is evaluated only by the mutual inductance $L_m$ and the internal resistances $r_1$ and $r_2$ of the coils from (8). The power transmitted to the secondary side in the SS circuit can be expressed as (11).

## 3. Analysis Parameters

**3.1. Litz wire resistance** All the power used for WPT is AC power. In the case of DC, we only need to consider the DC resistance of the conductor, but in the case of AC, we need to consider the AC resistance at the same time. In this section, we will derive the skin effect and proximity effect of copper loss, which are the main factors of AC resistance.

The skin effect loss is a loss that occurs under high-frequency conditions, where the current flowing in the conductor generates a magnetic field and eddy currents are generated in the conductor, causing the currents to cancel each other out, and the current flowing in the conductor is biased toward the skin part of the conductor. One of the countermeasures is to use a wire that is sufficiently thinner than the skin depth 1/e. With this countermeasure, the current flowing through the conductor can be 37% (1/e) or more of the conductor surface. [27–29]. The current flowing in the strand attenuates exponentially. In the 85 kHz band treated in this paper, the skin depth is about 0.225 mm, while a strand with a diameter of 0.05 mm is used, so a sufficiently thin strand can be used, and the advantages of Litz wire can be said to be utilized.

Next, proximity effect loss means that the magnetic field generated by the wire itself affects the neighboring wires, creating areas where it is difficult for the current to flow between the wires. In order to suppress proximity effect loss as much as possible, the twist structure and the twist pitch of Litz wire are important [30].

Litz wire, which is made up of many thin wires twisted together, is used to suppress AC resistance, but the proximity effect occurs because many wires are closely packed together in Litz wire. In general, Litz wire is often used in the kHz band because it is relatively easy to suppress copper loss, but in the MHz band, it is often difficult to select strands thinner than the skin depth in terms of cost and design difficulty, and single wires are often used because proximity effect loss and self-capacitance become dominant [31,32]. In recent years, Litz wire design in MHz band [33] has also been carried out. Thus, when handling AC, including WPT, it is necessary to carefully select a wire depending on the frequency band to be used.

In the Litz Wire, the skin effect and the proximity effect can be considered independently of each other. In addition, the internal magnetic field $H_i$ and the external magnetic field $H_e$, which are also factors of the proximity effect, are orthogonal to each other, so the resistance components can be evaluated separately [34].

Other losses that occur in AC include hysteresis loss and radiation loss, but these are ignored in this paper because the coil assumed in this paper has an empty core and the radiation loss is almost zero.

The equations to derive the skin effect loss and proximity effect loss are shown below [35]. The Litz wire parameters used are as shown in Fig. 4.

*Skin effect loss*:

$$P_{S,Litz} = n \cdot F_R(f) \cdot R_{DC} \cdot I_{rms}^2 \quad [\mathrm{W/m}] \tag{12}$$

*Proximity effect loss*:

$$P_{P,Litz} = n \cdot G_R(f) \cdot R_{DC} \cdot \left(H_e^2 + H_i^2\right) \quad [\mathrm{W/m}] \tag{13}$$

$n$, $\delta$, $R_{DC}$, $I_{rms}^2$, $F_R$ and $G_R$ are shown below.

$$\text{Number of Litz wire strands} : n$$

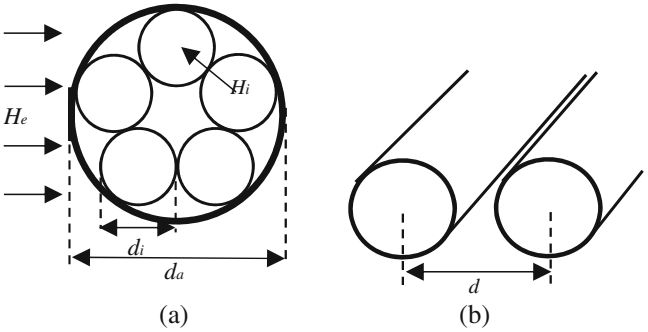


Fig. 4. Litz wire parameters. (a) External and internal magnetic fields (b) Pitch

$$\text{Epidermal depth} : \delta = \frac{1}{\sqrt{\pi \mu_0 \sigma f}}$$

$$\text{DC Resistance} : R_{DC} = \frac{4}{\sigma \pi d_i^2}$$

$$\xi = \frac{d_i}{\sqrt{2}\delta}$$

$$I_{rms}^2 = \frac{\widehat{I}^2}{2n^2}$$

$$F_R = \frac{\xi}{2\sqrt{2}} \cdot \frac{1}{\mathrm{ber}_1(\xi)^2 + \mathrm{bei}_1(\xi)^2} \cdot \{-\mathrm{ber}_0(\xi)\mathrm{ber}_1(\xi) + \mathrm{ber}_0(\xi)\mathrm{bei}_1(\xi) - \mathrm{bei}_0(\xi)\mathrm{ber}_1(\xi) - \mathrm{bei}_0(\xi)\mathrm{bei}_1(\xi)\}$$

$$G_R = -\frac{\xi \pi^2 di^2}{2\sqrt{2}} \cdot \frac{1}{\mathrm{ber}_0(\xi)^2 + \mathrm{bei}_0(\xi)^2} \cdot \{\mathrm{ber}_2(\xi)\mathrm{ber}_1(\xi) + \mathrm{ber}_2(\xi)\mathrm{bei}_1(\xi) - \mathrm{bei}_2(\xi)\mathrm{ber}_1(\xi) + \mathrm{bei}_2(\xi)\mathrm{bei}_1(\xi)\}$$

where $ber_n\ (x)$ and $bei_n\ (x)$ are $n$th-order Kelvin functions. $F_R$ and $G_R$ can also be obtained by applying cylindrical coordinates in Maxwell's equations [35]. This equation is for a round conductor, so if the shape is different, it is necessary to derive a new equation.

The external magnetic field $H_e$ is mainly determined by the winding pitch $d$ of the coil. Assuming that the adjacent wires are of infinite length and the current $\widehat{I}^2$ flows uniformly, it can be expressed by (14).

$$H_e^2 = \frac{\widehat{I}^2}{(2\pi d)^2} \tag{14}$$

For the internal magnetic field $H_i$, a numerical calculation method called the PEEC method (Partial Element Equivalent Circuit: PEEC) is used. The PEEC method is based on the integral equation of Maxwell's equations, where the conductive volume is subdivided into filaments along its length and cross-section, and the self-inductance and mutual inductance interact with each other, and each mesh is regarded as Kirchhoff's voltage law. Thus, the electromagnetic problem is reduced to the equivalent circuit problem [36]. As a result, the internal magnetic field $H_i$ can be accurately represented by numerical calculation.

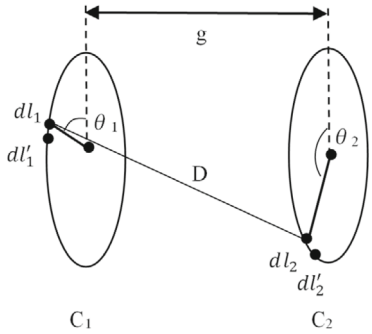


Fig. 5. Parameters of the Neumann equation

Finally, by dividing (12) and (13) by $\widehat{I}^2$, the AC resistance of the Litz wire, $r$ [Ω], can be expressed by (15) using the Litz wire length, $l$ [m], by combining the theoretical equation with numerical calculations.

$$r = \frac{\left(P_{S,Litz} + P_{P,Litz}\right)}{\widehat{I}^2} \cdot l \quad [\Omega] \tag{15}$$

**3.2. Mutual inductance** If there are coils on the transmission (primary side) and receiving (secondary side) sides, mutual inductance $L_m$ is generated between the coils, which can be derived by Neumann's equation (16) using the parameters in Fig. 5. Neumann equation is an absolute equation that does not depend on the frequency derived from the theory. However, at high frequencies where self-resonance occurs, the frequency dependence is clear from electromagnetic field analysis and experiments [37]

$$L_m = \frac{\mu_0}{4\pi} \oint_{C1} \oint_{C2} \frac{dl_1 dl_2}{D} \tag{16}$$

due to mutual capacitance between the two coils and the increase in resistance caused by the proximity effect, so care must be taken.

## 4. Optimization Procedure and Experiments

**4.1. Optimization procedure** The optimization procedure proposed in this paper is described in turn. A flowchart of the procedure is shown in Fig. 6.

*4.1.1. Determination of the assumed WPT environment* Determine the actual size of the coil to be designed. At the same time, determine the transmission distance and the applicable frequency band. As will be discussed later, due to the increase in the error of the PEEC method and the Neumann equation at high frequencies, the applicable frequency range of this method should be less than 200 kHz [35,36].

*4.1.2. Determine the Litz wire to be used* The strand diameter, the number of strands, and the twisting structure are determined in consideration of the applicable frequency band, the required allowable current, and the coil case. In order to reduce the skin resistance, the finer the strand diameter, the better, but if the number of strands increases, the DC resistance component and cost will increase, so it is necessary to select an appropriate one [30,31]. Regarding the twisting structure, it is necessary to be cautious in order to suppress the occurrence of skin effect and proximity effect not only at the strand level but also at the bundle level.

The effect of each on the Litz wire is shown in Fig. 7.

The number of strands that can be wound on the outermost bundle is shown in (17) using the skin depth $\delta$ and the strand diameter $d_i$.

$$n_{1,max} = \frac{4\delta^2}{d_i^2} \tag{17}$$

From this formula, at 85 kHz, e.g., the maximum number of strands is 20 when the strand diameter $d_i$ is 0.1 mm, and 80 strands when $d_i$ is 0.05 mm.

For the subsequent strands, it is important that all strands are twisted evenly with no gaps, so in the case of circular Litz wire, five strands or less is recommended [29]. As for the twisting pitch of each bundle, a longer pitch increases the proximity resistance at the strand level, while a shorter pitch increases the DC resistance and the proximity resistance at the strand level [24,36]. There are several references on the determination of the optimal twisting pitch, but it depends largely on the manufacturer.

*4.1.3. Determining the pitch between wires* The pitch is provided to suppress the proximity effect between wires and to increase the transmission power, but there is a trade-off: the wider the pitch, the smaller the inductance. In the case of kHz bands such as 85 kHz, the effect of the proximity effect is generally small, so the pitch is gradually increased from 0 mm.

*4.1.4. Line length expressed as number of turns* Once the pitch $d$ and the outline $d_a$ of the Litz wire used are determined, the line length $l$ can be expressed as a function of the number of turns $N$. In the case of this rectangular spiral coil, the winding is assumed to be perpendicular for simplicity, and can be expressed as (18) using the number of turns $N$, coil size $X$, $Y$, Litz wire outline $d_a$, and wire-to-wire gap $\alpha$ ($= d - d_a$).

$$l = \{2X + 2Y + 4\alpha - 4(d_a + \alpha) \cdot N\} \cdot N - \alpha \tag{18}$$

The parameters of the assumed rectangular coil are shown in Fig. 8.

*4.1.5. Correspondence between mutual inductance and number of turns* Find $N_{1max}$ and $N_{2max}$, which are the number of turns to wind the primary and secondary coils to the center, respectively, and obtain $L_{m,N1N2}$ ($N_1$: $1 \sim N_{1max}$, $N_2$: $1 \sim N_{2max}$).

*4.1.6. Internal resistance of Litz wire expressed as number of turns* Since the line length $l$ and the number of turns $N$ have been functionalized in the optimization procedure (Section 4.1.4), (15) can be expressed in terms of the number of turns $N$.

*4.1.7. Express the* kQ *product as a number of turns* In the proposed method, the $kQ$ product is obtained indirectly by the mutual inductance $L_m$ and the coil internal resistance $r$, as shown in (8). Since the mutual inductance $L_m$ and internal resistance $r$ can be expressed in terms of $N_1$ and $N_2$, the $kQ$ product, or maximum efficiency $\eta_{max}$, can both be expressed in terms of the number of turns $N_1$ and $N_2$ as shown below.

$$\textit{mutual inductance}: \quad L_m(N_1, N_2)$$

$$\textit{internal resistance}: \quad r_1(N_1), r_2(N_2)$$

$$kQ\ \textit{product}: \quad k^2 Q_1 Q_2 (N_1, N_2)$$

$$\textit{Maximum efficiency}: \quad \eta_{max}(N_1, N_2)$$

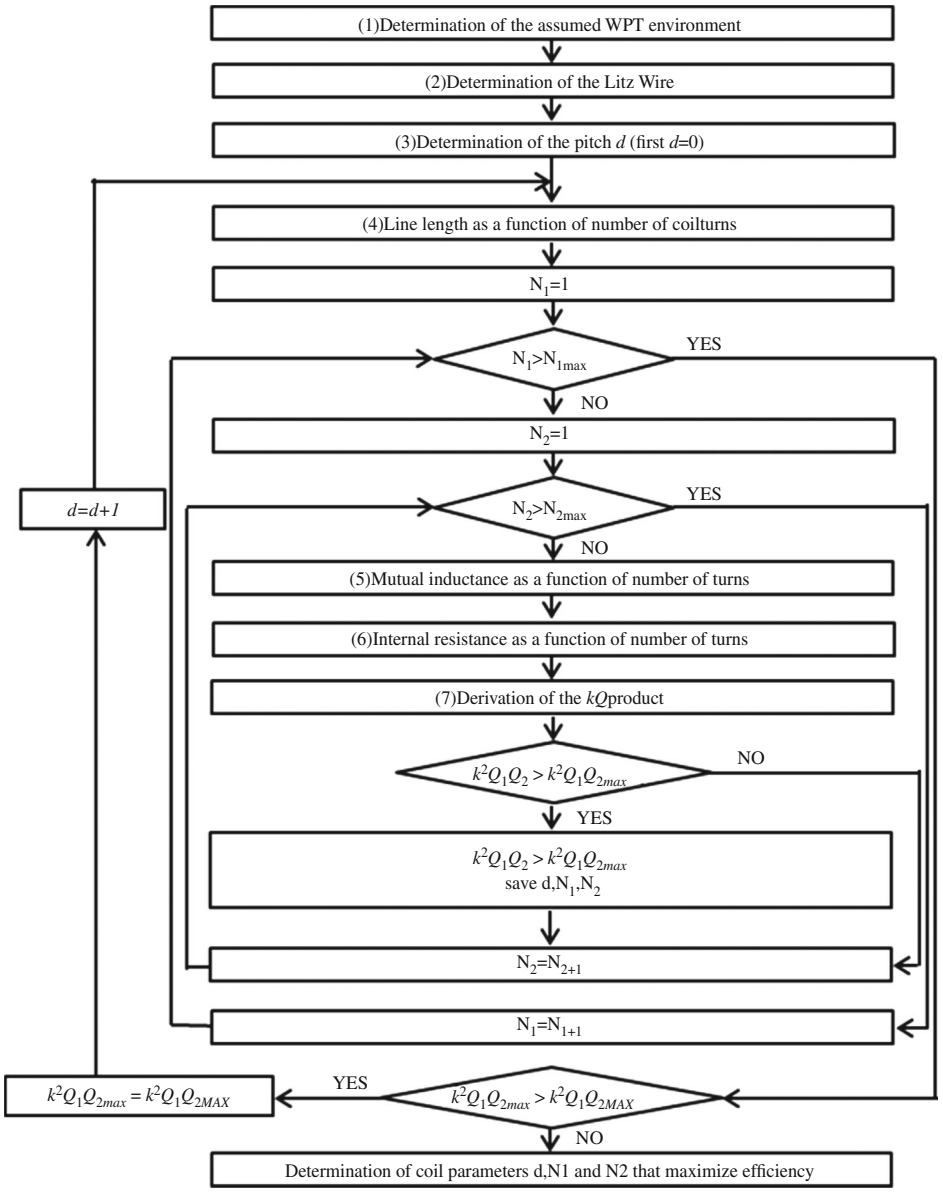


Fig. 6. Optimization procedure

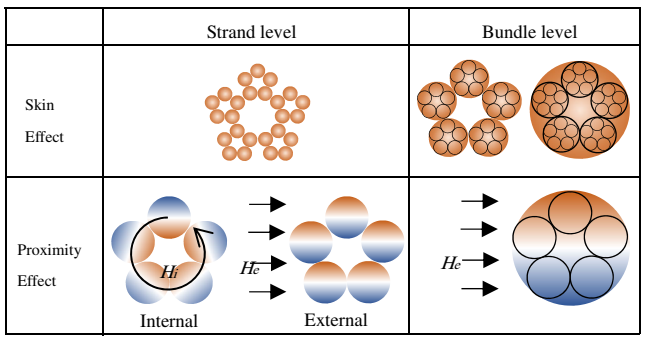


Fig. 7. Behavior of bundle-level and strand-level Litz wires

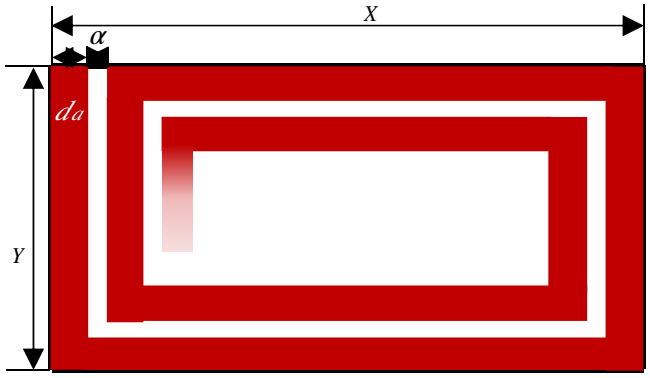


Fig. 8. Coil parameters. ($da$: Litz-wire diameter, $\alpha$: Distance between wire-to-wire ($=d-da$), $d$: Pitch (Fig. 4))

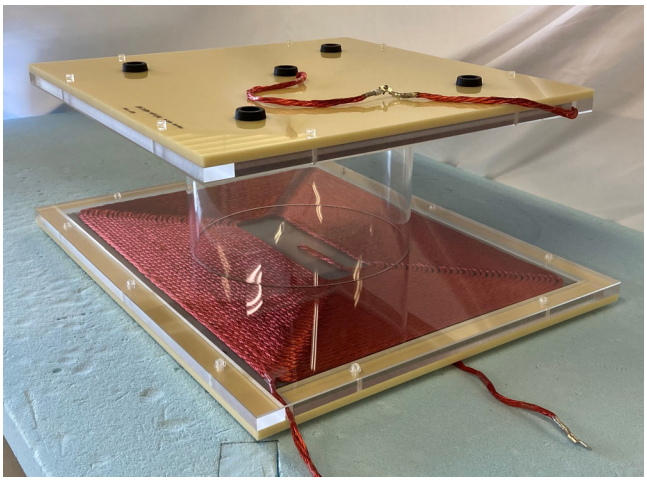

Fig. 9. Measurement scene

*4.1.8. Determining the optimal number of turns* Since the efficiency is a monotonic increase of the $kQ$ product from Fig. 3, we search for the combination of the number of turns $N_1$ on the transmission side and the number of turns $N_2$ on the receiving side that maximizes the $kQ$ product obtained in the optimization procedure (Section 4.1.7). For example, if the $N_{1max}$ and $N_{2max}$ of the primary and secondary sides are both 40 turns, a total of 1600 different $kQ$ products are obtained, and the combination of turns $N_1$ and $N_2$ with the maximum $kQ$ product is determined.

**4.2. Experiments** Following the proposed optimization procedure, we compare the analytical values with the measured values. In the measurement, we produced a coil with no gap between the Litz wires ($\alpha = 0$), which had the best transmission efficiency in the pitch selection described below. Figure 9 shows the measurement scene, Fig. 10 and Fig. 11 show the images of the created coil. An impedance analyzer (KEYSIGHT: E4990A) was used for the measurements.

*4.2.1. Determination of the assumed WPT environment* In this paper, the coils of Test station WPT1/Z3 shown in SAEJ2954 are used, and the transmission distance is set to 200 mm. Note that the transmission distance is strictly defined as the height from the ground to the receiving coil of the vehicle, but in this paper, it is the distance between the primary and secondary coils. The frequency was set to 85 kHz.

*4.2.2. Determine the Litz wire to be used* Assuming the specification of Litz wire with a strand diameter of 0.05 mm (AWG44), the resistance values were obtained simply for each number of strands using the proposed internal resistance analysis method. The strand diameter was chosen based on the trade-off between the strand diameter being sufficiently smaller than the skin depth $\delta$ and the design cost [31].

Figure 12 shows the relationship between the power to the optimum load $R_L$, $\eta_{max}$, and the maximum efficiency $\eta_{max}$ when the optimization is performed using Litz wires of various strand numbers. $\alpha = 0$ mm is used to find the coil with the highest efficiency within the specified coil size using each Litz wire, and the output power at this time. The line with 99% efficiency and the line with 3.7 kW output power are shown at the same time.

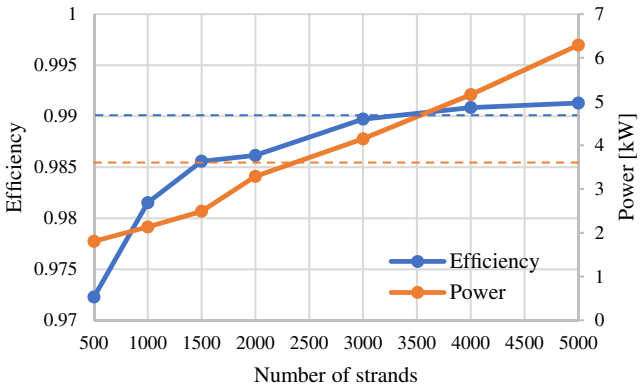


Fig. 12. Comparison of output power and efficiency against the number of strands

(a) (b) (c) (d) (e)

Fig. 10. Created transmission coil. (a) $N_1 = 40$. (b) $N_1 = 34$. (c) $N_1 = 30$. (d) $N_1 = 20$. (e) $N_1 = 4$

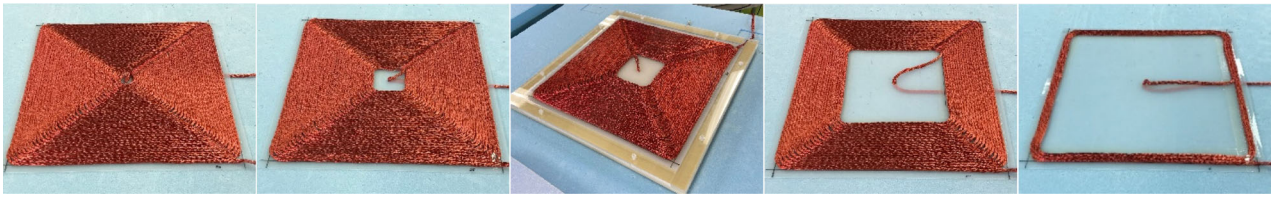

(a) (b) (c) (d) (e)

Fig. 11. Created receiving coil. (a) $N_2 = 40$ (b) $N_2 = 35$. (c) $N_2 = 30$. (d) $N_2 = 20$. (e) $N_2 = 3$

Table I. Parameters of the Litz wire used in the analysis

| Number of strands | Twisting structure | Twisting pitch (mm) | Litz wire outer diameter (mm) |
|---|---|---|---|
| 5000 | 40/5/5/5 | 50, 55, 70, 90 | 5.50 |
| 4000 | 32/5/5/5 | 50, 55, 70, 90 | 5.00 |
| 3000 | 24/5/5/5 | 50, 55, 70, 90 | 4.50 |
| 2000 | 80/5/5 | 50, 70, 90 | 4.00 |
| 1500 | 60/5/5 | 50, 70, 90 | 3.50 |
| 1000 | 50/5/4 | 50,70, 90 | 3.25 |
| 500 | 20/5/5 | 50, 70,90 | 3.00 |

The input voltage is 420 V AC in each case. However, since the Litz wire parameters used in the analysis need to be adjusted accordingly, the parameter values used are summarized in Table I. Increasing the number of strands lowers the resistance value and supports high power transmission by increasing the allowable current, but it leads to higher cost per length, so it is necessary to select the number of strands that suits the power to be transmitted and the current value that flows.

At around 4000 strands, the output power exceeded 3.7 kW, the efficiency exceeded 99%, and finally, the Litz wire used in the Test station shown in SAE J2954 has $d_a = 5$ mm, we concluded that 4000 strands of Litz wire was sufficient.

As for the stranding structure, we chose 32/5/5/5 according to (17).

*4.2.3. Determining the pitch between lines* The distance between the wires $\alpha$ is set to 0, 1, and 5 mm, respectively, and the following procedure is followed. To confirm the effect of pitch, the simulated values of $kQ$ product and efficiency are shown in Fig. 13 and Fig. 14. It can be seen that the highest $kQ$ product and the highest efficiency can be achieved when $\alpha = 0$ mm. The larger $\alpha$ is, the shorter the wire length used, and thus the smaller the internal resistance. On the other hand, even if the number of turns is the same, the magnetic flux crossing the loop is reduced, which leads to a decrease in inductance and coupling coefficient. Since the later effect is larger than the former, the $kQ$ product is considered to have decreased when $\alpha$ is increased. As the purpose of this paper is to maximize efficiency, it was set at $\alpha = 0$ mm.

*4.2.4. Line length expressed as number of turns* The parameters determined in Section 4.2.1–4.2.3 were substituted into (18).

*4.2.5. Derivation of mutual inductance* The mutual inductance was derived according to the Neumann equation for each number of turns of the primary and secondary side. Figure 15 shows the mutual inductance values for each turns on the transmission side when $N_2 = 30$. The analytical values and the measured values are in excellent agreement.

*4.2.6. Derivation of internal resistance* The resistance per unit length of Litz wire was determined by theoretical equation and numerical analysis. The coil resistance analyzed in Fig. 16 and Fig. 17 was compared with the measured value. As the number of turns increases, the error becomes larger, but this may be due to distortion of the actual winding, twisting misalignment, or for simplification, only the proximity effect of the Litz wire was considered, and parasitic capacitance was ignored. As explained in detail in the Appendix A, the increase in inductance causes the internal resistance of the coil to rise above the design value assuming that the coil has a parasitic capacitance.

In fact, the power receiving coil 40 turns and the 20 turns of the transmission coil have almost the same inductance. The slight distortion of the generated magnetic field due to the difference between the long and short sides of the rectangular coil may also have an effect.

Figure 18 shows the frequency characteristics when the receiving coil $N_2 = 30$. The reason why the error becomes larger as the frequency increases is thought to be because the PEEC method has an exponential error as the frequency increases, and the coil approaches its self-resonant frequency as the frequency increases when the effect of the parasitic capacitance of the coil is taken into account. We believe that this coil design method can be accurately proposed for frequencies below 200 kHz. It is said that it is

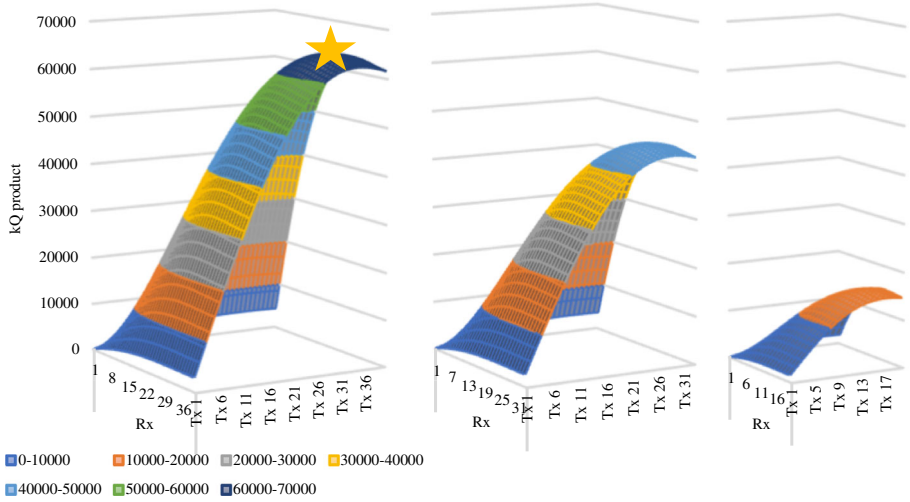


Fig. 13. $kQ$ product at each pitch (★: Peak of $kQ$ product [$N_1 = 34$, $N_2 = 30$]). (a) α = 0 (mm); (b) α = 1 (mm); (c) α = 5 (mm)

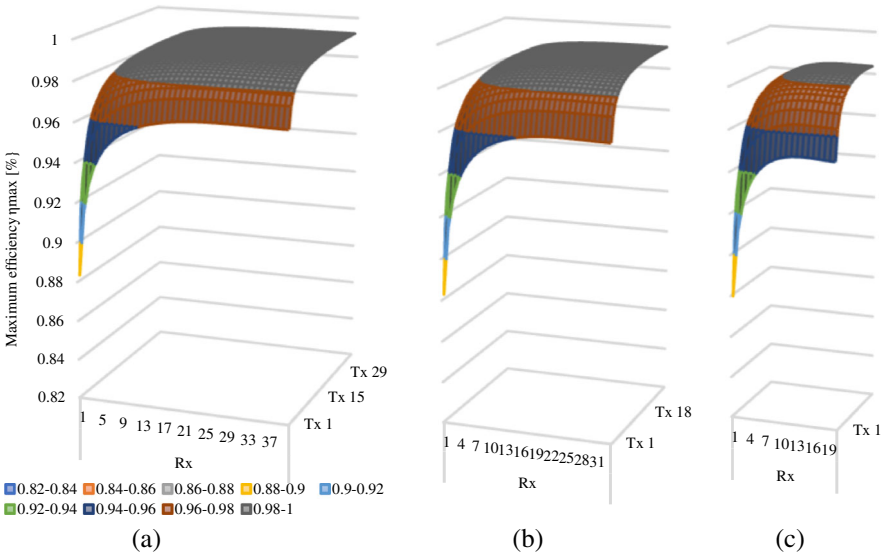


Fig. 14. Maximum efficiency $\eta_{max}$ at each pitch. (a) $\alpha = 0$ (mm); (b) $\alpha = 1$ (mm); (c) $\alpha = 5$ (mm)

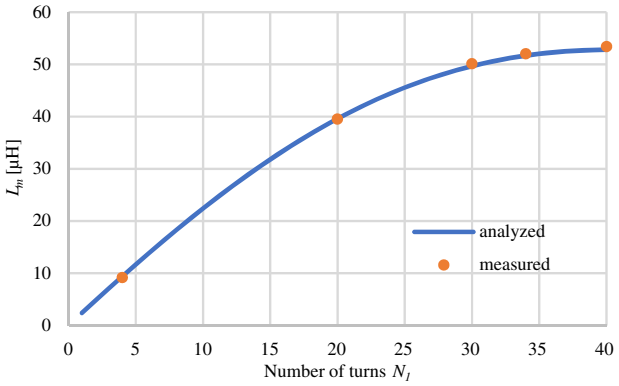


Fig. 15. Comparison between analyzed and measured values of mutual inductance $L_m$ ($N_2 = 30$)

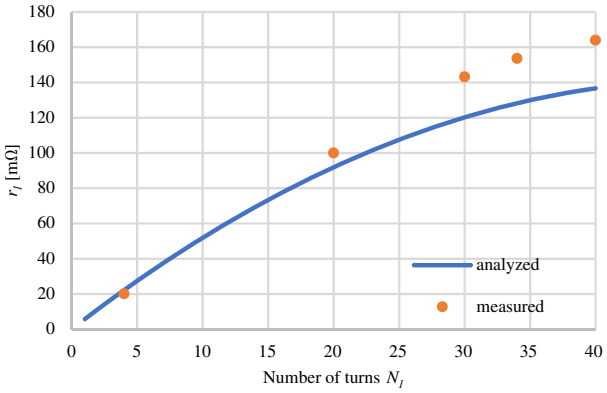


Fig. 16. Resistance of transmission coil

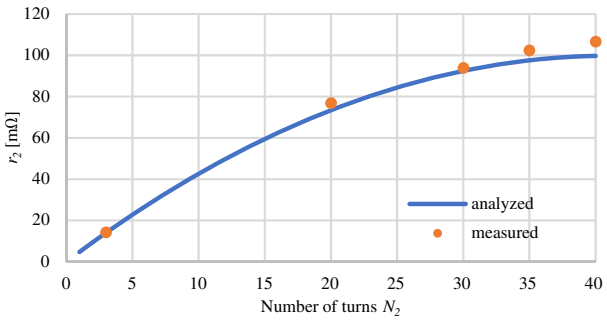


Fig. 17. Resistance of the receiving coil

difficult to predict the AC resistance of a coil, but the results in Fig. 16 and Fig. 17 capture the characteristics very well.

*4.2.7. Express the* kQ *product as a number of turns* Using the obtained mutual inductance $L_m$ ($N_1$,$N_2$), internal resistance $r_i$ (i = 1,2) and Equation (8), $k^2 Q_1 Q_2$ was obtained.

*4.2.8. Determining the optimal number of turns* In this paper, we calculated the $kQ$ product for 1600 different combinations of 40 turns on the transmission side and 40 turns on the receiving side, and determined the combination of turns with the peak $kQ$ product. Since it is difficult to visualize the evaluation in Fig. 13, Fig. 19, and Fig. 20 show the $kQ$ product and the efficiency $\eta_{max}$, respectively, with the number of turns on the transmission side fixed at $N_1 = 34$. In both cases, $N_1 = 34$ and $N_2 = 30$ was obtained as the optimum number of turns, which is consistent with the analysis. The efficiency is $\eta_{max} = 99.21\%$ in simulation and 99.13% in measurement. The highest efficiency was achieved although there was little difference in efficiency between the different numbers of turns. $kQ$ product shows a slight error when the number of turns is large, which is considered to be due to the error of the internal resistance of the coil. The error in Fig. 16 was about 20%, but the efficiency error was less than 0.1% compared with the measured value. This made it possible to design the optimum high-efficiency coil at a specific frequency and within a specific coil size.

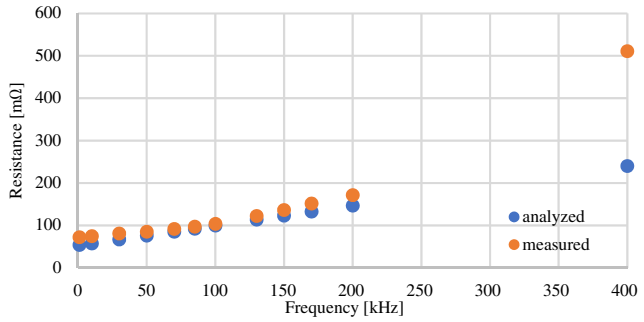


Fig. 18. Frequency response of resistance

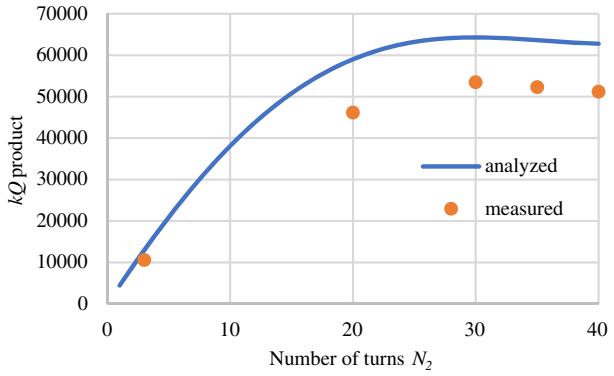


Fig. 19. $kQ$ product at each number of turns at 34 turns on the transmission side.

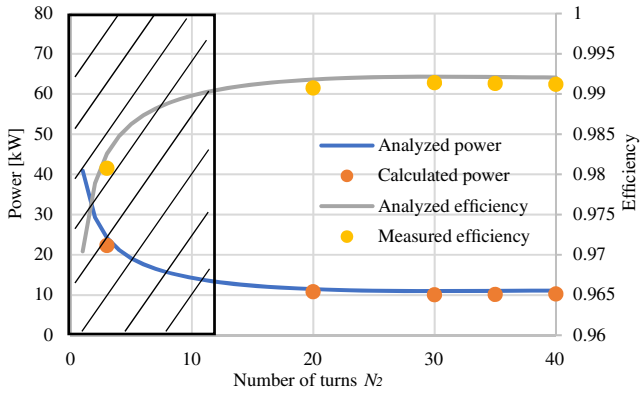


Fig. 20. Efficiency $\eta_{max}$ and output power $P2$ at number of turns at 34 turns on the transmission side. (The shaded area is the area where the allowable current of the Litz wire to be used is exceeded)

In WPT, it is important to obtain the desired power as well as the efficiency.

Figure 20 shows the relationship between the power and the number of turns. The trade-off between efficiency and power is shown in Fig. 21 shows the change in the current value with the change in the number of turns of the power receiving coil. Since the allowable current of the Litz wire used in this project is 38A, the area in where the allowable current of the Litz wire is reached when the input voltage is 600 V is shown with a shaded line. Since the purpose of this paper was to maximize efficiency, the distance $\alpha$ between the wires was set to 0 mm, but in order to obtain more

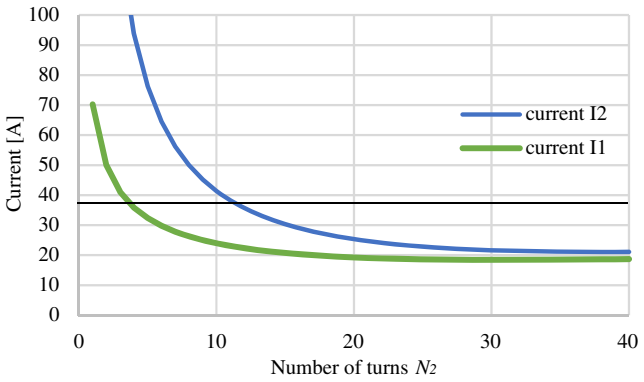


Fig. 21. Relationship between the number of turns on the receiving side and current values $I1$ and $I2$ at a point with the number of turns 34 on the transmission side

power, it is important to reduce the number of turns in the SS circuit, increase the distance $\alpha$ between the wires, and reduce the inductance.

## 5. Conclusion

In this paper, using theoretical equations and numerical analysis, we show how to derive the $kQ$ product indirectly by the internal resistance and mutual inductance of the coil, and how to obtain the transmission efficiency $\eta_{max}$ by the $kQ$ product. This makes it possible to design the optimum coil under the required coil size and other circumstances. As a result, an efficiency of 99.13% was obtained at a transmission distance of 200 mm when $N_1 = 34$ and $N_2 = 30$. Although this is a coil-to-coil efficiency, we believe it is very high for a coreless coil. The analysis of Litz wire with a large number of strands took about 24 h using a large computer for analysis, but once the resistance value per unit length of Litz wire to be used is determined, the analysis can be done in about 1 s per one coil combination using a laptop computer. This means that the design of WPT coils, regardless of whether they are for EVs or not, has become even more familiar. In addition, since electromagnetic field analysis is not performed, we were able to achieve highly accurate optimization while reducing time, labor, and cost. There was some error in the $kQ$ product, but the effect was negligible in terms of efficiency, and we were able to propose a highly efficient coil design method. At the same time, it was found that it is possible to design a coil that achieves the desired power. In this paper, the spacing $\alpha$ between the Litz wires was set to 0 mm, which is the environment where errors are most likely to occur. If the pitch is increased, it is thought that errors can be further reduced. Although the applicable frequency range is limited to a few hundred kHz or less, this makes it possible to propose the optimal coil within the required coil environment, and it is found to be useful for the infrastructure of EVs, which are expected to spread in the future. Prospects include optimization of ferrite installation, optimization of not only the coupler part but also the entire system, measures against magnetic field leakage, and evaluating the compatibility of various coils.

## Acknowledgment

This work was supported by JSPS KAKENHI Grant number 18H03768.

## Appendix A

### Consideration of the factors that caused the resistance error and the fact that this design method is limited to designs below 200 kHz

The cause of the error from the analysis value when the number of turns is increased, which occurred in Fig. 16, and the cause of the gradual increase in error at high frequencies above 200 kHz, which occurred in Fig. 18, are shown.

The ideal inductance is one in which the internal resistance can be neglected as shown in (a), but in AC, the internal resistance tends to be large. Therefore, in this research, the coil design has been carried out considering the internal resistance as shown in (b). In fact, however, it is necessary to consider the capacitance, which is a parasitic capacitance, along with the inductance and impedance as shown in (c) [37–39]. The impedance between terminals in Fig. A1 can be expressed as (A1). An approximation can be expressed by considering the units of the elements used for general WPT.

$$Z = \frac{R - j\left\{R^2\omega C + \omega^2 LC\left(\omega L - \frac{1}{\omega C}\right)\right\}}{\left(\omega^4 L^2 + \omega^2 R^2\right)C^2 - 2\omega^2 LC + 1}$$
$$\approx \frac{R - j\left\{R^2\omega C + \omega^2 LC\left(\omega L - \frac{1}{\omega C}\right)\right\}}{-2\omega^2 LC + 1} \quad \text{(A1)}$$

Looking at the error generation in Fig. 16 and Fig. 17, it can be seen that the error becomes larger as the number of turns increases. The magnitude of the error in Fig. 16 is larger than that in Fig. 17. This can be explained by (A1), which shows that the larger the inductance, the higher the resistance value tends to be. From Fig. 16 and Fig. 17, it can be seen that the error of the coil with $N1 = 20$ is close to that of the coil with $N2 = 40$. The inductance of the receiving coil when $N2 = 40$ is 296 μH in actual measurement, while the inductance when $N1 = 40$ is 452 μH. On the other hand, the inductance of the coil when $N1 = 20$ is 262 μH. The inductance is very close, and the error between the two is close, so the validity of the consideration can be said.

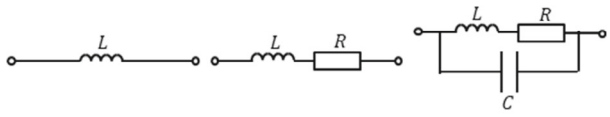


(a) (b) (c)

Fig. A1. Equivalent circuit of the coil used

Next, in Fig. 18, the error spreads gradually as the frequency increases. It can be seen from (A1) that the denominator becomes smaller as the frequency increases, leading to an increase in the resistance value.

The parasitic capacitance is mainly divided into the one generated between the windings of the Litz wire and the one generated between the Litz wire and the ground or core. The coil made in this study has a distance $\alpha$ of 0 mm between the Litz wires; widening $\alpha$ can significantly reduce the parasitic capacitance [38]. When the distance between the wires is increased, the inductance is lowered even with the same number of turns, and the parasitic capacitance is reduced, so it is thought that a more accurate design is possible.

An accurate model for estimating the parasitic capacitance has not yet been established except by electromagnetic field analysis, and this paper is therefore limited to design methods in the frequency band well below the self-resonant frequency of coils below 200 kHz.

## References


(1) Kurs A, Karalis A, Moffatt R, Joannopoulos JD, Fisher P, Soljacic M. Wireless power transfer via strongly coupled magnetic resonances. *Science* 2007; **317**(5834):83–86.

(2) Patil D, McDonough MK, Miller JM, Fahimi B, Balsara PT. Wireless power transfer for vehicular applications: Overview and challenges. *IEEE Transactions on Transportation Electrification* 2018; **4**(1):3–37.

(3) Yilmaz M, Krein PT. Review of battery charger topologies, charging power levels, and infrastructure for plug-in electric and hybrid vehicles. *IEEE Transactions on Power Electronics* 2013; **28**(5):2151–2169. https://doi.org/10.1109/TPEL.20.

(4) K. Sasaki, T. Imura, Combination of sensorless energized section switching system and double-LCC for DWPT. 2020 *IEEE PELS Workshop on Emerging Technologies; Wireless Power Transfer (WoW)*, 2020.

(5) Tavakoli R, Pantic Z. Analysis design and demonstration of a 25-kW dynamic wireless charging system for roadway electric vehicles. *IEEE Journal of Emerging and Selected Topics in Power Electronics* 2018; **6**:1378–1393.

(6) Jang YJ, Jeong S, Ko YD. System optimization of the on-line electric vehicle operating in a closed environment. *Computers and Industrial Engineering* 2015; **80**:222–235.

(7) Onar OC, Miller JM, Campbell SL, Coomer C, White CP, Seiber LE. A novel wireless power transfer for in-motion EV/PHEV charging. In *Twenty-Eighth Annual IEEE Applied Power Electronics Conference and Exposition (APEC)*. Long Beach: CA; 2013.

(8) H. Fujimoto, O. Shimizu, S. Nagai, T. Fujita, D. Gunji and Y. Ohmori, Development of Wireless In-wheel Motors for Dynamic Charging: From 2nd to 3rd generation. *IEEE PELS Workshop on Emerging Technologies: Wireless Power (WoW), Korea*, pp. 56–61, 2020.

(9) Thackeray MM, Wolvertonb C, Isaacs ED. Electrical energy storage for transportation—Approaching the limits of, and going beyond, lithium-ion batteries. *Energy & Environmental Science* 2012; **5**:7854–7863.

(10) Kim SW, Seo DH, Ma X, Ceder G, Kang K. Electrode materials for rechargeable sodium-ion batteries: Potential alternatives to current lithium-ion batteries. *Advanced Energy Materials* 2012; **2**(7):710–721.

(11) P. D. Aghcheghloo, D. J. Wilson and T. Larkin, Towards the Electrification of Road Infrastructure. Equity in Transportation, New Zealand, 2020.

(12) Arias MB, Bae S. Electric vehicle charging demand forecasting model based on big data technologies. *Applied Energy* 2016; **183**:327–339.

(13) Ji B, Hata K, Imura T, Hori Y, Shimada S, Kawasaki O. Wireless power transfer system design with power management strategy control for lunar rover. *IEEJ Journal of Industry Applications* 2020; **9**(4):392–400.

(14) Z. Huang, I. W. Iam, I. U. Hoi, C. Lam, P. Mak and R. P. Martins, Self-Contained Solar-Powered Inductive Power Transfer System for Wireless Electric Vehicle Charging. *IEEE PES Asia-Pacific Power And Energy Engineering Conference (APPEEC)*, Macao 2019.

(15) Mohamed AAS, Lashway CR, Mohammed O. Modeling and feasibility analysis of quasi-dynamic WPT system for EV applications. *IEEE Transactions on Transportation Electrification* 2017; **3**(2):343–353.

(16) Li S, Mi CC. Wireless power transfer for electric vehicle applications. *IEEE Journal of Emerging and Selected Topics in Power Electronics* 2015; **3**(1):4–17.

(17) K. W. Klontz, D. M. Divan, D. W. Novotny and R. D. Lorenz, Contactless battery charging system. US Patent 5157319, 1991.
(18) Wang C-S, Stielau OH, Covic GA. Design considerations for a contactless electric vehicle battery charger. *IEEE Transactions on Industrial Electronics* 2005; **52**(5):1308–1314.
(19) X. Nan and C. R. Sullivan, An improved calculation of proximity-effect loss in high-frequency windings of round conductors. *Power Electronics Specialist Conference 2003. PESC'03* pp. 853–860 2003.
(20) Bosshard R, Kolar JW. Multi-objective optimization of 50 kW/85 kHz IPT system for public transport. *IEEE Journal of Emerging and Selected Topics in Power Electronics* 2016; **4**:1370–1382.
(21) Mizuno T, Enoki S, Asahina T, Suzuki T, Noda M, Shinagawa H. Reduction of proximity effect in coil using Magnetoplated wire. *IEEE Transactions on Magnetics* 2007; **43**(6):2654–2656.
(22) Namadmalan A, Jaafari B, Iqbal A, Al-Hitmi M. Design optimization of inductive power transfer systems considering bifurcation and equivalent AC resistance for spiral coils. *IEEE Access* 2020; **8**:141584–141593.
(23) D. Barth, B. Klaus and T. Leibfried, Litz wire design for wireless power transfer in electric vehicles. *Proceedings under IEEE Wireless Power Transfer Conference* (WPTC), pp. 1–4, 2017.
(24) C. R. Sullvian and Richard Y. Zhang, Analytical model for effects of twisting on Litz-wire losses. *2014 IEEE 15th workshop on control and modeling for power electronics (COMPEL)*, 2014.
(25) T. Noda, T. Nagashima and H. Sekiya, A design of inductively coupled wireless power transfer system with coupling coil optimization. *Proceedings of the IEEE International Telecommunications Energy Conference*, pp. 1–6, 2015.
(26) SAE International, "Wireless Power Transfer for Light-Duty Plug-in/Electric Vehicles and Alignment Methodology J2954," 2020.
(27) Imura T. *Wireless Power Transfer: Using Magnetic and Electric Resonance Coupling Techniques*. Springer: Singapore; 2020.
(28) Sullivan CR. Optimal choice for number of strands in a litz-wire transformer winding. *IEEE Transactions on Power Electronics* 1999; **14**(2):283–291.
(29) C. R. Sullivan and R. Y. Zhang, Simplified design method for litz wire. *IEEE Applied Power Electronics Conference and Exposition* (APEC), pp. 2667–2674,. 2014.
(30) Sullivan CR. Cost-constrained selection of strand wire and number in a Litz-wire transformer winding. *IEEE Transactions on Power Electronics* 2001; **16**:281–288.
(31) J. Cho, J. Sun, H. Kim, J. Fan, Y. Lu and S. Pan, Coil design for 100 KHz and 6.78 MHz WPT system: Litz and solid wires and winding methods. *2017 IEEE International Symposium on Electromagnetic Compatibility & Signal/Power Integrity (EMCSI)*.
(32) B. A. Reese, R. Joseph and C. R. Sullivan, 2018 Improved litz-wire designs for the MHz range. *IEEE 19th Workshop on Control and Modeling for Power Electronics (COMPEL)*, pp. 1–8, .
(33) Ferreira JA. Analytical computation of AC resistance of round and rectangular litz wire windings. *IEE Proceedings B (Electric Power Applications)* 1992; **139**(1):21–25.
(34) Mühlethaler J. Modeling and multi-objective optimization of inductive power components. *DIS.ETH* 2012; **20217**:223.
(35) Richard Y. Zhang, Jacob K. White, and John G. Kassakian, Charles R. Sullivan, Realistic Litz Wire Characterization Using Fast Numerical Simulations. *Applied Power Electronics Conference and Exposition*, pp.738–745, 2014.
(36) Raju S, Wu R, Chan M, Yue CP. Modeling of mutual coupling between planar inductors in wireless power applications. *IEEE Transactions on Power Electronics* 2014; **29**(1):481–490.
(37) Dalessandro L, da Silveira Cavalcante F, Kolar JW. Self-capacitance of high-voltage transformers. *IEEE Transactions on Power Electronics* 2007; **22**(5):2081–2092.
(38) Grandi G, Kazimierczuk MK, Massarini A, Reggiani U. Stray capacitances of single-layer solenoid air-core inductors. *IEEE Transactions on Industry Applications* 1999; **35**(5):1162–1168.
(39) Mosleh ME, Besmi MR. Stray capacitance of a magneto cumulative generator including $N$-turn, single-layer, solid, and round conductor with insulating coating. *IEEE Transactions on Plasma Science* 2011; **39**(10):1990–1997.

**Yuto Yamada** (Student Member) He entered the Department of Electrical Engineering, Faculty of Science and Technology, Tokyo University of Science in April 2017, graduated in March 2021, and entered the Department of Electrical Engineering, Graduate School of Science and Technology, Tokyo University of Science in April 2021. He is currently focusing on the design of coils for wireless power supply to electric vehicles and the realization of Dynamic Wireless Power Transfer. He is a student member of the Institute of Electrical and Electronics Engineers (IEEE) and the Institute of Electrical Engineers of Japan (IEEJ).

**Takehiro Imura** (Member) Received the bachelor's degree in electrical and electronics engineering from Sophia University, Tokyo, Japan, in 2005, and the M.E. degree in electronic engineering and the D.Eng. degree in electrical engineering from The University of Tokyo, Tokyo, in 2007 and 2010, respectively. He joined the Department of Advanced Energy, Graduate School of Frontier Sciences, University of Tokyo, as a Research Associate, where since 2015, he has been a Project Lecturer. In 2019, he joined the Department of Electrical Engineering, Tokyo University of Science, as an Associate Professor. He is currently investigating wireless power transfer using magnetic resonant coupling and electric resonant coupling. His research interests include electric vehicle in-motion connected to renewable energy, sensors, and cancer treatment. He is the winner of the IEEJ Industry Applications Society Distinguished Transaction Paper Award in 2015, of the IEEE Power Electronics Transactions First Prize Paper Award in 2017. He is a member of the Institute of Electrical and Electronics Engineers (IEEE), the Institute of Electronics, Information and Communication Engineers (IEICE), and the Society of Automotive Engineers of Japan (JSAE).